


## Theoretical velocity of an object frictionally coupled to a two-mode vibrating plate

Xiaolin Zhang, Timothy C. Hui, William D. Ristenpart<sup>✉, \*</sup> and Gregory H. Miller<sup>†</sup>  
 Department of Chemical Engineering, University of California, Davis, California 95616, USA

 (Received 23 February 2024; accepted 1 August 2024; published 19 August 2024)

Net velocity has been demonstrated for objects frictionally coupled to a flat plate that oscillates periodically in-plane with two frequencies, provided plate displacement is nonantiperiodic: the ratio of frequencies  $\gamma$  cannot be the ratio of two odd integers. We give a mathematical derivation of the experimentally determined dependence of mean velocity on the relative amplitudes of the two frequency modes, and the phase lag between the modes, when  $\gamma = 2$ , and when the magnitude of plate acceleration is much larger than the magnitude of acceleration by static friction. The approach uses an analysis of the symmetry properties of the roots of trigonometric polynomials, without explicit determination of those roots. The behavior when  $\gamma = 1/2$ , and specific phase lags that inhibit net velocity for general  $\gamma$ , are also determined.

DOI: [10.1103/PhysRevE.110.024212](https://doi.org/10.1103/PhysRevE.110.024212)

### I. INTRODUCTION

As reviewed by Denisov *et al.* [1], the nonantiperiodic [2] excitation of nonlinear systems is a ratchetlike mechanism for promoting transport. This concept has been applied to microscopic, optical, and quantum systems [3–14], and also to macroscopic objects [15–24], where it has application to material handling. Vidybida and Serikov developed a predictive analysis of general induced motion when the nonlinear restorative force is Lipschitz continuous [25]. In this paper, we analyze frictional coupling, where the restorative force lacks this continuity. Umbanhowar and Lynch [23] developed and validated an analytical model for frictional motion induced by a discontinuously accelerated surface. Here we prove an experimentally validated [18] simple closed-form analytical solution to the harmonic two-mode continuously driven friction problem for certain ranges of parameters in an easily accessible regime. Our proof provides a firm theoretical foundation for the predictive design of new processes for the transport of solids, including the use of solid reagents in so-called laboratory-on-a-chip devices.

We are concerned with the vibratory motion of a horizontal flat surface, displaced in-plane in one dimension with two frequencies of ratio  $\gamma$ ,

$$x(t) = A \sin(\omega t) + B \sin(\gamma \omega t + \phi),$$

and a single object sitting on the surface, accelerated by static and kinetic friction,

$$\dot{v} = \begin{cases} \ddot{x}, & v = \dot{x} \text{ and } |\ddot{x}| < \mu_s g \text{ (sticking)} \\ \mu_k g \operatorname{sgn}(\dot{x} - v) & \text{otherwise (sliding)}. \end{cases}$$

Here,  $v$  is the velocity of the object,  $\mu_s$  is the coefficient of static friction,  $\mu_k$  is the coefficient of kinetic friction,  $g$

is gravitational acceleration, and  $\operatorname{sgn}$  is the signum function [ $\operatorname{sgn}(0) = 0$ , otherwise  $\operatorname{sgn}(x) = x/|x| = \pm 1$ ]. Figure 1 illustrates how this can be achieved with consumer-grade audio equipment. See Hui *et al.* [18] for experimental details.

In dimensionless variables,

$$\begin{aligned} s(\tau) &= \sin(\tau) + \beta \sin(\gamma \tau + \phi), \\ \dot{u}(\tau) &= \begin{cases} \dot{s}, & u = \dot{s} \text{ and } |\dot{s}| < \frac{1}{\operatorname{Fr}_s} \text{ (sticking)} \\ \frac{\operatorname{sgn}(\dot{s} - u)}{\operatorname{Fr}_k} & \text{otherwise (sliding)}, \end{cases} \end{aligned} \quad (1)$$

where  $s = x/A$ ,  $\beta = B/A$ ,  $\tau = \omega t$ ,  $u = v/(A\omega)$ , and  $\operatorname{Fr}_s = A\omega^2/(\mu_s g)$  is the “static friction number,” which characterizes the relative magnitudes of the driving and static frictional accelerations acting on the object, and  $\operatorname{Fr}_k = A\omega^2/(\mu_k g)$  is the kinetic friction number.

### II. RESULTS

The system has spatial symmetry: the ordinary differential equation (ODE) is invariant with respect to any in-plane translation. If  $s(\tau)$  had only a single frequency (i.e.,  $\beta = 0$ ), there would be a temporal symmetry too and there would be no net motion ( $\langle u \rangle = 0$ ). When there are two driving frequencies ( $\beta \neq 0$ ), Hashemi *et al.* [17] proved that  $s(\tau)$  is antiperiodic [2] if  $\gamma$  is the ratio of two odd integers. When this temporal symmetry applies, again there is no net motion. However, if  $\gamma$  can be reduced to being even/odd or odd/even, antiperiodicity is lost: the symmetry constraint is broken and net motion may occur if  $\beta \neq 0$ . The system then acts as a sort of temporal ratchet [26].

If  $\beta \neq 0$  and  $\gamma$  is irrational, then  $s(\tau)$  is not periodic. The sliding object may be observed to have either net positive or net negative motion, depending on the observation window.

When  $\operatorname{Fr}_s$  is large, the dynamics (1) converge to a unique limit cycle (for constant  $\gamma, \beta, \phi$ ), which collapses to a fixed point in the  $(u, \dot{u})$  phase space when  $\operatorname{Fr}_s \rightarrow \infty$ .

With forcing  $s(\tau)$  being periodic, the response  $u(\tau)$  will also be periodic at the steady state,  $\langle \dot{u} \rangle = 0$ , and therefore if

\*Contact author: [wdristenpart@ucdavis.edu](mailto:wdristenpart@ucdavis.edu)

†Contact author: [grgmiller@ucdavis.edu](mailto:grgmiller@ucdavis.edu)

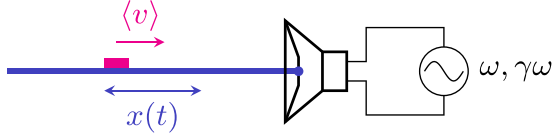


FIG. 1. A horizontal surface (blue) is attached to a stationary audio speaker driven with a two-frequency ac signal. The surface vibrates (displacement  $x$ ) but has no net motion. An object placed on the platform (magenta) is accelerated by frictional coupling. Its mean velocity  $\langle v \rangle$  may be nonzero.

sticking does not occur,

$$\int_0^T \text{sgn}[\dot{s}(\tau) - u(\tau)] d\tau = 0,$$

where  $T$  is the dimensionless period. Sticking does not occur, or has a negligible effect, when  $\text{Fr}_s \rightarrow \infty$  because the fraction of the period when  $|\dot{s}| < 1/\text{Fr}_s$  is vanishingly small. Recalling that  $\text{Fr}_k > \text{Fr}_s$  because  $\mu_s > \mu_k$ , in the large- $\text{Fr}_s$  limit,  $|\dot{u}|$  will also be negligible,  $u \rightarrow \langle u \rangle$ . In this limit, the average velocity  $\langle u \rangle$  is determined by setting to zero the mean acceleration by kinetic friction. Then,  $\langle u \rangle$  is the zero of the function

$$f(\langle u \rangle) = \int_0^T \text{sgn}[\dot{s}(\tau) - \langle u \rangle] d\tau. \quad (2)$$

When (2) is zero,  $\dot{s} > \langle u \rangle$  over half the period and  $\dot{s} < \langle u \rangle$  over the other half. For continuous  $\dot{s}$ ,  $f$  is strictly monotonically decreasing in the range of  $\dot{s}$ . Surprisingly, the mean velocity predicted by (2) is independent of all frictional properties of the system.

Numerical determination of the root of (2) uses Newton's method with bisection as a fallback. The integral is evaluated by first finding all points  $\tau_i$  that satisfy

$$\langle u \rangle = \dot{s}(\tau_i), \quad (3)$$

using bracketing and iterative refinement, then summing the signed distances between these points.

When  $\text{Fr}_s$  is finite, a different numerical solution may be constructed by solving the dynamical equations (1) as a boundary value problem, using periodicity as the boundary condition. Numerical exploration of this more complicated approach reveals that when  $\text{Fr}_s \gtrsim 7$ , the value of  $\langle u \rangle$  computed from (2) deviates from the boundary value calculation by  $\lesssim 10\%$  for any  $\beta$  (see Supplemental Material [28, Sec. 1]). As  $\beta$  increases from  $1/4$ , the requisite  $\text{Fr}_s$  decreases. Thus, although the limit  $\text{Fr}_s \rightarrow \infty$  is not physically realizable, the properties of the simpler equation (2) reveal the essential properties of the more general solution for large ( $\gtrsim 7$ , depending on  $\beta$ ) but finite  $\text{Fr}_s$ . In this paper, we focus on solutions of (2).

By numerical investigation of (2), we deduced that when  $\text{Fr}_s$  is large and  $\gamma = 2$ ,

$$\langle u \rangle = \begin{cases} -2\beta \cos(\phi), & |\beta| \leq 1/4 \\ -\cos(\phi)/(8\beta), & |\beta| > 1/4. \end{cases} \quad (4a)$$

$$(4b)$$

Reznik and Canny [21] discovered the equivalent of (4a) for any  $\phi$ , and the equivalent of (4b) when  $\phi = 0$  [using a displacement  $s(\tau)$  depending on cosines instead of sines]. They

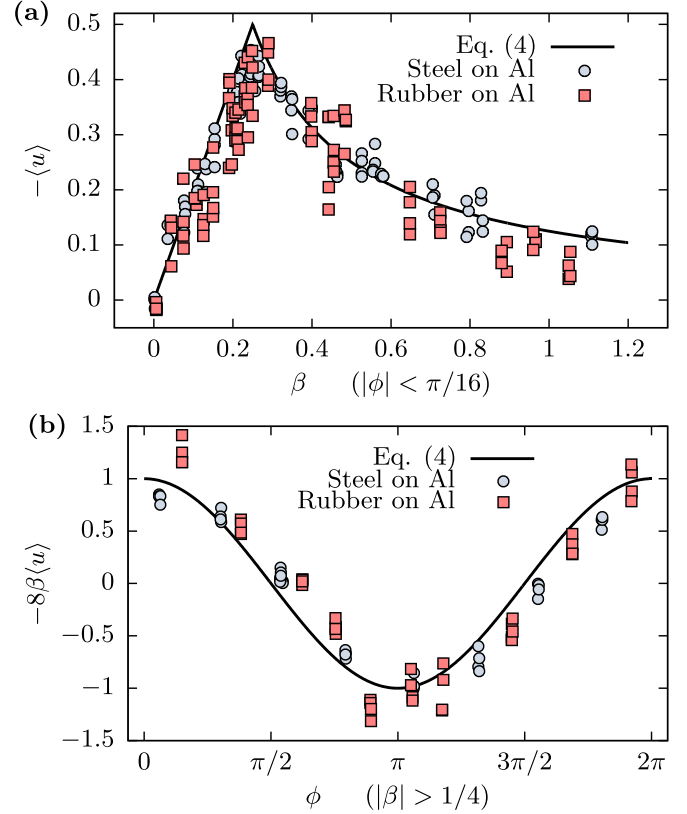


FIG. 2. Experimental validation of (4). (a) The piecewise  $\beta$  dependence when  $\gamma = 2$ ,  $\phi = 0$ , and  $\omega/2\pi = 30$  Hz.  $\text{Fr}_s$  ranges are 2.9–13.8 (steel) and 3.9–11.7 (rubber). (b) The  $\cos(\phi)$  dependence with  $\gamma = 2$  and  $\omega/2\pi = 30$  Hz.  $\text{Fr}_s$  ranges are 3.0–3.6 (steel) and 5.7–7.5 (rubber), and  $\beta$  ranges are 0.43–0.48 (steel) and 0.40–0.44 (rubber). Friction coefficients were measured using an inclined plane [27]; kinetic coefficients were determined by measuring particle location with high-speed video, and fitting to a parabola. For steel on aluminum,  $\mu_s = 0.338 \pm 0.017$  and  $\mu_k = 0.337 \pm 0.039$ , and for rubber on aluminum,  $\mu_s = 0.375 \pm 0.014$  and  $\mu_k = 0.365 \pm 0.022$ . Reported errors are  $\pm 1\sigma$  from 10 replicates.

further noted that the same  $\phi$  that makes  $\langle u \rangle$  zero for small  $|\beta|$  makes  $\langle u \rangle$  zero for large  $|\beta|$ . The complete formula (4) is derived below.

There is no net motion when  $\text{Fr}_s$  is large and  $\phi = \pm\pi/2$ . We have experimentally validated this relation for simple sliding objects, such as steel and rubber washers (Fig. 2; see, also, Supplemental Material [28, Sec. 1]). Although colliding, rolling objects such as sand or dry yeast aggregates are subject to additional forces, we also find qualitative agreement between the motion of such granular materials and this simple theory [18].

To prove (4) when  $\gamma = 2$ , and when  $\text{Fr}_s$  is large such that (2) is applicable, the strategy is to find values of  $\langle u \rangle$  that yield points of intersection  $\tau_i$  (3) that partition the period  $T = 2\pi$  to make (2) be zero. Figure 3 illustrates how the character of the solution changes with  $\beta$ . When  $|\beta| < 1/4$ , there is one root at  $\pi/2$  and another at  $-\pi/2$ , independent of  $\beta$  and  $\phi$ . When  $|\beta| = 1/4$ , a degenerate root pair appears at a  $\phi$ -dependent time, and when  $|\beta| > 1/4$ , there are four asymmetrically distributed roots that partition the period.

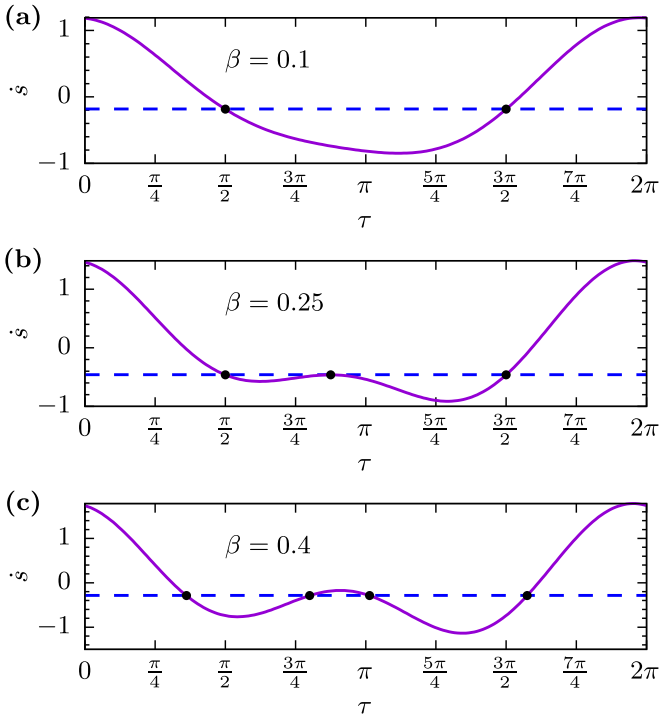


FIG. 3. The solution  $\langle u \rangle$  (blue dashed line) to  $f = 0$  [cf. Eq. (2)] in response to surface motion  $\dot{s}$  (purple curve) with  $\gamma = 2$ ,  $\phi = \pi/8$ : (a) when  $\beta = 0.1$ , two roots (filled circles) at  $\pi/2$  and  $3\pi/2$  separate the domain into two equal pieces; (b) when  $\beta = 0.25$ , a degenerate root appears at  $\pi - \phi$ ; and (c) when  $\beta = 0.4$ , there are four roots asymmetrically distributed.

First observe that for any  $\beta$ ,

$$\dot{s}\left(\pm\frac{\pi}{2}\right) = \cos\left(\pm\frac{\pi}{2}\right) + 2\beta\cos(\pm\pi + \phi) = -2\beta\cos(\phi). \quad (5)$$

If  $\langle u \rangle = -2\beta\cos(\phi)$ , then (3) gives two zeros,  $\pm\pi/2$ : they partition the period into two intervals of length  $\pi$ . When  $|\beta| < 1/4$ , these are the only real zeros of (3) (see Supplemental Material [28, Sec. 2]), and therefore (2) is zero when  $\langle u \rangle = -2\beta\cos(\phi)$  and  $|\beta| < 1/4$ . When  $|\beta| = 1/4$ , a new degenerate root appears, but because it has multiplicity 2, or 3 if  $\phi = \pm\pi/2$ ,  $\text{sgn}(\dot{s} - \langle u \rangle)$  does not change value across the degenerate point and (2) is still zero. Equation (4a) is proved. This same analysis can be applied to any  $\gamma = 2n$ , with  $n$  an integer, with the result that

$$\langle u \rangle = (-1)^n \gamma \beta \cos(\phi),$$

if  $|\beta|$  is sufficiently small. To study the case  $|\beta| > 1/4$  when  $\gamma = 2$ , it is convenient to express (3) in the complex plane using the change of variables,  $z = \exp(i\tau)$ , with  $i = \sqrt{-1}$ . Then, (3) becomes

$$0 = z^4 + z^3 \frac{e^{-i\phi}}{2\beta} - z^2 \frac{\langle u \rangle e^{-i\phi}}{\beta} + z \frac{e^{-i\phi}}{2\beta} + e^{-2i\phi}, \quad (6a)$$

for which we desire the factorization

$$0 = [z^2 + z\mathcal{O}(\beta^{-1}) - ie^{-i\phi}][z^2 + z\mathcal{O}(\beta^{-1}) + ie^{-i\phi}]. \quad (6b)$$

In the limit  $|\beta| \rightarrow \infty$ , the roots of (6b) are easily found: expressed as dimensionless times, they are  $\pi/4 - \phi/2$  and

$5\pi/4 - \phi/2$  from the first factor, and  $3\pi/4 - \phi/2$  and  $7\pi/4 - \phi/2$  from the second. Importantly, the roots of the first factor are interleaved with those of the second. If this proposed factoring is achieved, from the first factor one has  $z_1 z_3 = -i \exp(-i\phi)$  for any  $\beta$ , and from the second factor one has  $z_2 z_4 = i \exp(-i\phi)$ . Together,

$$\frac{z_1 z_3}{z_2 z_4} = -1 = e^{\pi i}. \quad (7)$$

Taking the argument of both sides,

$$(\tau_1 - \tau_4) + (\tau_3 - \tau_2) = \pi,$$

which makes (2) zero; see Fig. 4(a). To achieve this factoring, compare the expanded (6a) and factored (6b) expressions to obtain three equations (for the coefficients of  $z$ ,  $z^2$ , and  $z^3$ ) in three unknowns [ $\langle u \rangle$  and the two  $z\mathcal{O}(\beta^{-1})$  terms]. Solving this algebraic system determines  $\langle u \rangle = -\cos(\phi)/(8\beta)$  (see Supplemental Material [28, Sec. 3]).

The proposed factorization (6b) is necessary and sufficient to determine the unique  $\langle u \rangle$  that zeros (2) in the limit  $|\beta| \rightarrow \infty$ . To prove (4b), it is also necessary to show that the roots of the two factors remain interleaved for all  $|\beta| > 1/4$ . Because the roots are interleaved in time at  $\infty$  and because they are continuous functions of  $\beta$ , they remain interleaved in time as  $|\beta|$  decreases until a degeneracy occurs. In the  $|\beta|$  interval  $[1/4, \infty)$ , the only degenerate point is  $|\beta| = 1/4$  (see Supplemental Material [28, Sec. 4]) (Fig. 5); Eq. (4b) is proved. This approach can be extended to other  $\gamma$  cases, although the algebra becomes increasingly cumbersome as the number of roots increases [29]. When  $\gamma = 4$ , one finds  $\langle u \rangle = -\cos(\phi)/(2^{12}\beta^3)$  in the limit  $|\beta| \rightarrow \infty$ .

Nonzero net motion is only found when  $\gamma$  is the ratio of an even and an odd integer [17]. We have discovered numerically that when  $\phi = \pm\pi/2$  and  $\gamma$  is even/odd, then  $\langle u \rangle = 0$  for all  $\beta$ , as found in the special case  $\gamma = 2/1$ . However, if  $\gamma$  is odd/even, then the mean velocity need not be zero when  $\phi = \pm\pi/2$ . Physically, when  $\gamma$  is even/odd and  $\phi = \pm\pi/2$ , the roots of (3) are partitioned in a way that causes the net motion to be zero. This condition (like  $\beta = 0$  and  $\gamma = \text{odd/odd}$ ) provides a temporal symmetry constraint. If any of these constraints is active, there is no net motion. If none of these constraints apply, net motion is possible but not required (see, e.g., Fig. 2(e) of [17]).

First we show that  $\langle u \rangle = 0$  is always the solution to (2) when  $\text{Fr}_s$  is large,  $\phi = \pm\pi/2$ , and  $\gamma = n/m$  is even/odd. If the ratio  $n/m$  is reduced, the period  $T$  is  $2\pi m$ . Let  $\hat{\tau} = \tau/m$ , so that  $-\pi \leq \hat{\tau} \leq \pi$  in the period. The root-determining condition of zero net motion (3) becomes

$$0 = \cos(m\hat{\tau}) \mp \gamma \beta \sin(n\hat{\tau}). \quad (8)$$

Expressing these trigonometric functions in terms of  $\sin(\hat{\tau})$  and  $\cos(\hat{\tau})$  using de Moivre's theorem with the binomial theorem (see Supplemental Material [28, Sec. 5]), one finds

$$\cos(\hat{\tau})P_{m-1}[\sin(\hat{\tau})] = \pm \gamma \beta \cos(\hat{\tau})Q_{n-1}[\sin(\hat{\tau})], \quad (9)$$

where  $P_{m-1}$  and  $Q_{n-1}$  are polynomials of degree  $m-1$  and  $n-1$ , respectively. One set of roots is  $\hat{\tau} = \pm\pi/2$ , from the  $\cos(\hat{\tau})$  factors on either side of the equation. Then, factoring out  $\cos(\hat{\tau})$ , the remaining roots come from a polynomial in  $\sin(\hat{\tau})$ : for every root  $\hat{\tau}$ , there will be a mirror root at  $\pi - \hat{\tau}$ .

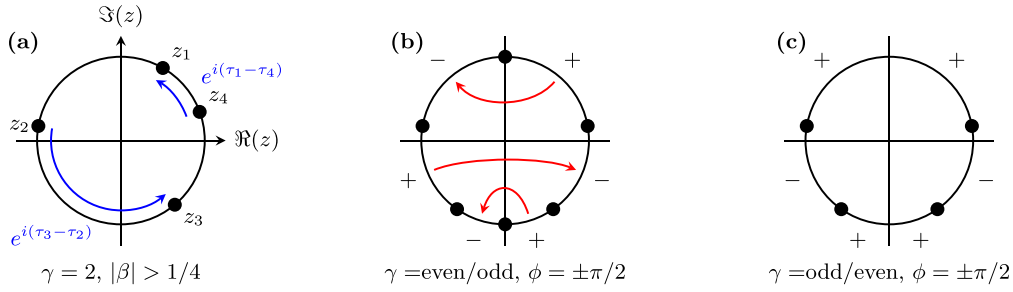


FIG. 4. Cartoons representing the relation between roots (filled circles) on a unit circle. (a) Roots  $t_i$  of (6b) as points  $z_i$  on the complex unit circle. The sum of the 41 and 23 arc lengths, the argument of  $z_1 z_2 / z_3 z_4$ , is half the period:  $\pi$ . (b) Symmetry relations for the roots of  $0 = \dot{s}$  when  $\gamma$  is even/odd and  $\phi = \pm\pi/2$ , constructed by treating dimensionless time  $\hat{\tau}$  as an angle measured clockwise from the positive horizontal axis. Alternating signs of the  $\text{sgn}$  function are indicated by  $+$  and  $-$ . Because of roots at  $\pm\pi/2$  and because of the left-right symmetry of the other roots, the signs are antisymmetric, guaranteeing that (2) is zero. (c) Symmetry relations for the roots of  $0 = \dot{s}$  when  $\gamma$  is odd/even and  $\phi = \pm\pi/2$ . Because the roots display left-right symmetry, but there are no roots at  $\pm\pi/2$ , the signs are not antisymmetric. A zero average velocity is possible but not assured.

The symmetry of these roots about the unit circle proves that they partition the period into sets of equal length, making (2) zero; see Fig. 4(b). Degeneracy at  $\pm\pi/2$  could spoil the solution, but it may be shown that only one of the roots  $\pm\pi/2$  can be degenerate, and it will have multiplicity 3 (see Supplemental Material [28, Sec. 6]):  $\dot{s}$  will change sign, and the symmetry-dictated solution  $\langle u \rangle = 0$  remains valid.

Now consider the case that  $\gamma = n/m$  is odd/even. Again, the period is  $2\pi m$  if  $n/m$  is reduced, and we change variables to  $\hat{\tau} = \tau/m$ . If the mean velocity is zero, then (8) again applies, but now de Moivre and the binomial theorem give

$$P_m[\sin(\hat{\tau})] = \mp \beta \gamma Q_n[\sin(\hat{\tau})].$$

As before, for every root in the right half-plane, there is a mirror root in the left half-plane, but there cannot be sign changes at either  $\pi/2$  or  $-\pi/2$  (see Supplemental Material [28, Sec. 5]). In this case, the roots may partition the period into sets of equal length, making (2) zero, but it is not required. This construction is illustrated in Fig. 4(c).

One observation that has so far defied quantitative explanation is the distribution of mean velocities as a function of  $\beta, \gamma, \phi$ , e.g., Fig. 6. This figure shows the special character of the  $\gamma = 2$  case, where  $\langle u \rangle \neq 0$  unless  $\beta = 0$ . Aside from vertical stripes for special values of  $\gamma$ , there is also a distinct

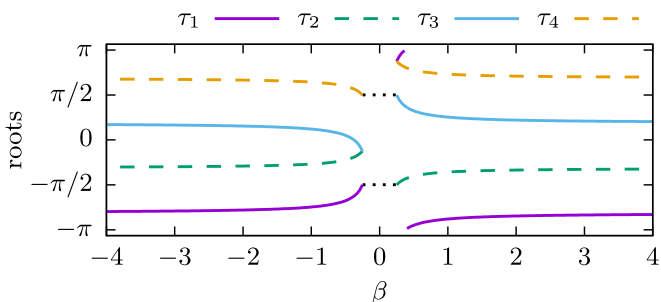


FIG. 5. The four roots of (3) as times, computed with  $\phi = \pi/8$ , maintain consistent ordering except at  $\beta = \pm 1/4$ . Roots of the first factor of (7b) (solid) and roots of the second factor (dashed) are interleaved, which is critical to the interpretation of (8). When  $|\beta| < 1/4$ , the roots are  $\pm\pi/2$  (black, dotted) from (6).

$\beta \gamma \approx 1$  trend. With

$$\dot{s} = \cos(\tau) + \beta \gamma \cos(\gamma \tau),$$

the surface velocity has a single mode when  $\beta \gamma = 0$  or when  $\beta \gamma \rightarrow \pm\infty$ , and  $\langle u \rangle$  will be zero in those limits. Evidently, the interplay of the two modes, which is essential to the observation of net motion, is greatest when  $\beta \gamma = \mathcal{O}(1)$ . This qualitative observation is consistent with the points in Fig. 6 clustering near the  $\beta \gamma = 1$  curve, but does not explain why they are denser below the curve when  $\gamma > 1$  and above the curve when  $\gamma < 1$ . The behavior when  $\gamma < 1$  is related to the behavior when  $\gamma > 1$  by a rescaling (see Supplemental Material [28, Sec. 7]). In general,

$$\langle u \rangle(\gamma^{-1}, \beta^{-1}, -\phi/\gamma) = \frac{1}{\beta \gamma} \langle u \rangle(\gamma, \beta, \phi),$$

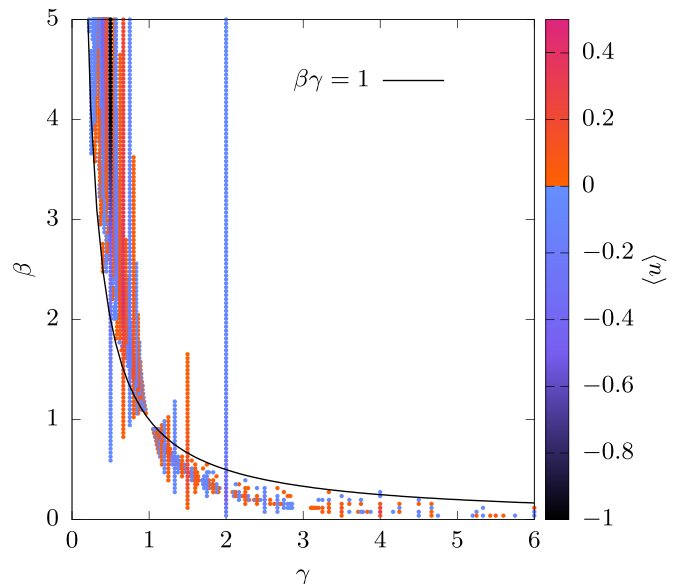


FIG. 6. Numerically computed values of  $\langle u \rangle$  with  $\phi = 0$ , where  $\gamma = n/m$  is a ratio of integers with  $m \in [1, 63]$ . Only  $|\langle u \rangle| > 0.02$  values are shown. Points are sorted so that large  $|\langle u \rangle|$  values are plotted above smaller overlapping ones.

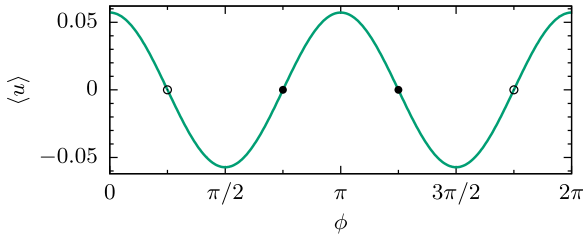


FIG. 7. The dependence of  $\langle u \rangle$  on  $\phi$  when  $\gamma = 3/2$  and  $\beta = 1$ , calculated numerically from (4), with zeros predicted from the symmetry of the complementary  $\gamma = 2/3$  problem to be at  $\pm 3\pi/4$  (filled circles), and two additional roots at  $\pm\pi/4$  (open circles) offset by  $\pi$ .

and, in particular, rescaling (4) gives

$$\langle u \rangle(1/2, \beta, \phi) = \begin{cases} -\beta^2 \cos(2\phi)/16, & |\beta| < 4 \\ -\cos(2\phi), & |\beta| \geq 4. \end{cases} \quad (10)$$

Equation (10) suggests that our chosen scaling gives larger dimensionless velocities when  $\gamma < 1$  than when  $\gamma > 1$ , and thereby explains the apparent greater density of high velocity values plotted in Fig. 6 when  $\gamma < 1$ . Sampling bias accounts for the greater density of  $\gamma < 1$  points tested, but does not account for the disparity of plotted velocity values.

This scaling argument predicts that  $\langle u \rangle(1/2n, \beta, \phi) = (-1)^n \cos(2n\phi)$  for integer  $n$  in the limit  $|\beta| \rightarrow \infty$ , where (3) has two real roots in period  $T = 4n\pi$ , and  $\langle u \rangle(1/4, \beta, \phi) = -\beta^4 \cos(4\phi)/2^{14}$  in the limit  $|\beta| \rightarrow 0$ , where (3) has eight real roots in  $T = 8\pi$ .

This analysis also suggests that the symmetry-mandated mean velocity zeros found when  $\phi = \pm\pi/2$  and  $\gamma$  is even/odd predict zeros in the complementary odd/even case,  $\gamma' = 1/\gamma$ , when the phase lag  $\phi'$  is  $\pm\pi\gamma'/2$ . Changing the phase lag by  $\pi$  is like changing the sign of  $\beta$ , which will not affect the symmetry zeros. Therefore, when  $\gamma'$  is odd/even, additional zeros are expected at  $\pm\pi\gamma'/2 \pm \pi$ . Figure 7 shows that  $\pm\pi\gamma'/2$  and  $\pm\pi\gamma'/2 \pm \pi$  accounts for the four observed  $\phi$  roots of the odd/even case  $3/2$ .

The preceding results all strongly suggest that the system behavior is deterministic, but a natural question is whether chaotic behavior can be observed. The answer is no in the large-Fr limit of interest here. First, the Poincaré-Bendixson theorem precludes the existence of strange attractors because the phase space of our ODE is two dimensional. Second, in the limit  $\text{Fr} \rightarrow \infty$ ,  $u(\tau) = \langle u \rangle$ , a constant; and the monotonicity of Eq. (2) makes the  $\langle u \rangle$  solution, hence  $u(\tau)$ , unique. Therefore, period doubling, a route to chaotic behavior, cannot occur. However, when Fr is finite, period doubling might occur and chaotic behavior may be possible. Our preliminary numerical searches through the large parameter space ( $\gamma, \beta, \phi, \text{Fr}_s, \text{Fr}_k$ ) have not found evidence of period doubling. Detailed numerical results for finite Fr are left to future investigations.

### III. CONCLUSIONS

In conclusion, a mathematical analysis of the large-Fr<sub>s</sub> formula (2) proves the numerically discovered, experimentally verified formula (4) when the frequency ratio  $\gamma$  is 2. Comparing the substrate velocity with ratio  $\gamma$  to the same motion with ratio  $1/\gamma$  gives a complementary result for the case  $\gamma = 1/2$ , given by Eq. (10). If  $\gamma$  is the ratio of an even to an odd integer, the mean velocity  $\langle u \rangle$  is zero when the phase lag  $\phi$  is  $\pm\pi/2$ . When  $\gamma$  is the ratio of odd to even integers, symmetry does not require  $\langle u \rangle = 0$  when  $\phi = \pm\pi/2$ . But, appealing to the relation between  $\gamma$  dependence and  $1/\gamma$  dependence, symmetry-dictated zeros are deduced at  $\phi = \pm\pi\gamma/2$  and  $\pm\pi\gamma/2 \pm \pi$ . We offer a qualitative justification for large nonzero  $\langle u \rangle$  values lying near the curve  $\gamma\beta = 1$ , and results (4) and (10) explain the existence of certain special values of  $\gamma$  for which significant mean velocities are found for almost every  $\beta$ . However, the distribution of large velocities in the  $\gamma, \beta, \phi$  parameter space remains largely unexplained.

### ACKNOWLEDGMENT

This material is based upon work supported by the National Science Foundation under Grant No. CBET-2125806.

- 
- [1] S. Denisov, S. Flach, and P. Hänggi, Tunable transport with broken space-time symmetries, *Phys. Rep.* **538**, 77 (2014).
- [2] The second half period of an antisymmetric or shift symmetric function is the negative of the first:  $f(t) = -f(t + T/2)$ , where  $T$  is the period.
- [3] S. Denisov, S. Flach, A. A. Ovchinnikov, O. Yevtushenko, and Y. Zolotaryuk, Broken space-time symmetries and mechanisms of rectification of ac fields by nonlinear (non)adiabatic response, *Phys. Rev. E* **66**, 041104 (2002).
- [4] S. Denisov, L. Morales-Molina, and S. Flach, Quantum resonances and rectification in ac-driven ratchets, *Europhys. Lett.* **79**, 10007 (2007).
- [5] S. Denisov, L. Morales-Molina, S. Flach, and P. Hänggi, Periodically driven quantum ratchets: Symmetries and resonances, *Phys. Rev. A* **75**, 063424 (2007).
- [6] A. S. Dukhin and S. S. Dukhin, Aperiodic capillary electrophoresis method using an alternating current electric field for separation of macromolecules, *Electrophoresis* **26**, 2149 (2005).
- [7] A. Eckardt, Colloquium: Atomic quantum gases in periodically driven optical lattices, *Rev. Mod. Phys.* **89**, 011004 (2017).
- [8] S. Flach, O. Yevtushenko, and Y. Zolotaryuk, Direct current due to broken time-space symmetry, *Phys. Rev. Lett.* **84**, 2358 (2000).
- [9] R. Gommers, S. Bergamini, and F. Renzoni, Dissipation-inducing symmetry breaking in a driven optical lattice, *Phys. Rev. Lett.* **95**, 073003 (2005).
- [10] R. Gommers, S. Denisov, and F. Renzoni, Quasiperiodically driven ratchets for cold atoms, *Phys. Rev. Lett.* **96**, 240604 (2006).
- [11] P. H. Jones, M. Goonasekera, and F. Renzoni, Rectifying fluctuations in an optical lattice, *Phys. Rev. Lett.* **93**, 073904 (2004).
- [12] M. Schiavoni, L. Sanchez-Palencia, F. Renzoni, and G. Grynberg, Phase control of directed diffusion in a

- symmetric optical lattice, *Phys. Rev. Lett.* **90**, 094101 (2003).
- [13] J. Struck, C. Ölschläger, M. Weinberg, P. Hauke, J. Simonet, A. Eckardt, M. Lewenstein, K. Sengstock, and P. Windpassinger, Tunable gauge potential for neutral and spinless particles in driven optical lattices, *Phys. Rev. Lett.* **108**, 225304 (2012).
- [14] A. V. Ustinov, C. Coqui, A. Kemp, Y. Zolotaryuk, and M. Salerno, Ratchetlike dynamics of fluxons in annular Josephson junctions driven by biharmonic microwave fields, *Phys. Rev. Lett.* **93**, 087001 (2004).
- [15] A. Buguin, F. Brochard, and P.-G. de Gennes, Motions induced by asymmetric vibrations, *Eur. Phys. J. E* **19**, 31 (2006).
- [16] D. Fleishman, Y. Asscher, and M. Urbakh, Directed transport induced by asymmetric surface vibrations: Making use of friction, *J. Phys.: Condens. Matter* **19**, 096004 (2007).
- [17] A. Hashemi, M. Tahernia, T. C. Hui, W. D. Ristenpart, and G. H. Miller, Net motion induced by nonantiperiodic vibratory or electrophoretic excitations with zero time average, *Phys. Rev. E* **105**, 065001 (2022).
- [18] T. C. Hui, X. Zhang, D. Adiga, G. H. Miller, and W. D. Ristenpart, Vibrational manipulation of dry granular materials in lab-on-a-chip devices, *Lab Chip* **24**, 966 (2024).
- [19] J. Nath, S. Das, A. Vishwakarma, and A. DasGupta, Directed transport of a particle on a horizontal surface under asymmetric vibrations, *Physica D* **440**, 133452 (2022).
- [20] A. E. Quaid, A miniature mobile parts feeder: Operating principles and simulation results, in *Proceedings of the 1999 IEEE International Conference on Robotics and Automation (Cat. No. 99CH36288C)* (Institute for Electrical & Electronics Engineers, Detroit, MI, USA, 1999), Vol. 3, pp. 2221–2226.
- [21] D. S. Reznik and J. F. Canny, The Coulomb pump: A novel parts feeding method using a horizontally-vibrating surface, in *Proceedings. 1998 IEEE International Conference on Robotics and Automation (Cat. No.98CH36146)* (Institute of Electrical & Electronics Engineers, Leuven, Belgium, 1998), Vol. 1, pp. 869–874.
- [22] D. S. Reznik and J. F. Canny, A flat rigid plate is a universal planar manipulator, in *Proceedings. 1998 IEEE International Conference on Robotics and Automation (Cat. No.98CH36146)* (Institute of Electrical & Electronics Engineers, Leuven, Belgium, 1998), Vol. 2, pp. 1471–1477.
- [23] P. Umbanhowar and K. M. Lynch, Optimal vibratory stick-slip transport, *IEEE Trans. Automat. Sci. Eng.* **5**, 537 (2008).
- [24] C. Viswarupachari, A. DasGupta, and S. P. Khastgir, Vibration induced direct transport of particles, *J. Vib. Acoust.* **134**, 051005 (2012).
- [25] A. K. Vidybida and A. A. Serikov, Electrophoresis by alternating fields in a non-Newtonian fluid, *Phys. Lett. A* **108**, 170 (1985).
- [26] A. Hashemi, E. T. Gilman, and A. S. Khair, A multiple-timing analysis of temporal ratcheting, *Eur. Phys. J. E* **47**, 28 (2024).
- [27] T. Kelemenová, M. Dovica, P. Božek, I. Koláriková, O. Benedik, I. Virgala, E. Prada, L. Miková, T. Kot, and M. Kelemen, Specific problems in measurement of coefficient of friction using variable incidence tribometer, *Symmetry* **12**, 1235 (2020).
- [28] See Supplemental Material at <http://link.aps.org/supplemental/10.1103/PhysRevE.110.024212> for results demonstrating the approach to  $\text{Fr} \rightarrow \infty$ , and for proofs of some mathematical statements.
- [29] When  $\gamma = 2n$ , with  $n$  a positive integer, the factorization template is  $0 = (z^{2n} + \dots - ie^{-i\phi})(z^{2n} + \dots + ie^{-i\phi})$ . Including  $\langle u \rangle$ , there are  $4n - 1$  variables.